anisms of the reaction of 1 with $Co_2(CO)_8$, $Fe_2(CO)_9$, and $Re_2(CO)_{10}$. We believe both reactions are initiated by an overall cycloaddition between the $Ta{=}CH_2$ group of 1 and a CO ligand of the dinuclear metal carbonyl complex. After this step, the pathways apparently diverge, as suggested in Figs. 2 and 3. The Re reaction appears to be a Wittig-type interaction between a CO ligand and a $M{=}CH_2$ group in which the carbon and oxygen atoms are simply interchanged to form a vinylidene ligand.

Our experiments record new examples of reactions in homogeneous solution between early and late transition metal complexes. These processes result in overall transformations in which CO molecules are coupled to one another and to CH_2 ligands, in one case with cleavage of the CO bond and accompanying rearrangement of hydrogen on the CH_2 groups. The rapid occurrence of these reactions appears to be a direct result of the interaction of two metal complexes in which the metal centers have very different electronic properties. It is not yet known whether transformations exhibiting related types of cleavage and rearrangement on surfaces (such as the Fischer-Tropsch process which forms alcohols, ketones, or aldehydes from CO and H_2) proceed by mechanisms similar to those involved in the reactions described here. However, the potential analogies are interesting. We hope that our results stimulate further studies of chemical interactions between early and late transition metal carbon-containing species in both homogeneous and heterogeneous media so that the similarities and differences between processes occurring under these two conditions may be better understood.

REFERENCES AND NOTES

1. M. van der Reit, D. Copperthwaite, R. Hunter, G. J. Hutchings, *J. Chem. Soc. Chem. Commun.* **1988**, 512 (1988).
2. G. A. Somorjai, *Chemistry in Two Dimensions: Surfaces* (Cornell Univ. Press, Ithaca, NY, 1981).
3. J. E. Bercaw, R. D. Sanner, D. R. McAlister, J. M. Manriquez, *J. Am. Chem. Soc.* **100**, 2716 (1978).
4. C. D. Wood and R. R. Schrock, *ibid.* **101**, 5421 (1979).
5. E. M. Carnahan and S. J. Lippard, *ibid.* **114**, 4166 (1992), and references cited there.
6. R. V. Anslyn, B. D. Santarsiero, R. H. Grubbs, *Organometallics* **7**, 2137 (1988).
7. D. R. Neithamer *et al.*, *J. Am. Chem. Soc.* **111**, 9056 (1989).
8. R. Toreki, R. E. LaPointe, P. T. Wolczanski, *ibid.* **109**, 7558 (1987).
9. R. R. Schrock, *ibid.* **97**, 6577 (1975).
10. Nuclear magnetic resonance (NMR) data for $Cp_2(CH_3)Ta(C_3H_2O_2)Fe_2(CO)_7$ (**3**): ^1H NMR (THF-d_8): δ 6.12 (5H, s, Cp); 6.11 (5H, s, Cp); 2.55 (1H, d, $J = 5.2$, CH_2); 1.63 (1H, d, $J = 5.2$, CH_2); and 0.85 (1H, s, CH_3). ^{13}C NMR (THF-d_8): δ 214.19 (s, CO); 198.40 (s, CO); 189.30 (s, CO); 144.43 (s, μ-CO); 112.72 (m, Cp); 112.61 (m, Cp); 100.48 (s, μ_2-C_2O_2); 89.20 (s, μ_2-C_2O_2); 39.65 (t, $J_{CH} = 157$, CH_2); and 36.38 (q, $J_{CH} = 128$, CH_3).
11. NMR data for $Cp_2(CH_3)Ta(C_3H_2O_2)Co_2(CO)_6$ (**2**): ^1H NMR (C_6D_6): δ 5.23 (5H, s, Cp); 5.09 (5H, s, Cp); 3.12 (1H, d, $J = 2.5$, CH_2); 2.49 (1H, d, $J = 2.6$, CH_2); and 0.65 (3H, s, CH_3). $^{13}C\{^1H\}$ NMR (THF-d_8): δ 208.97 (s); 207.81 (s); 207.64 (s); 204.18 (s); 139.04 (s); 129.04 (s); 112.92 (s); 112.85 (s); 49.18 (s); and 36.75 (s).
12. Phosphine-substituted uranium carbene complexes have been shown to undergo a similar reaction with dinuclear iron carbonyls; compare with J. W. Gilje and R. E. Cramer, *Inorg. Chim. Acta* **139**, 177 (1987).
13. R. E. Cramer, K. T. Higa, S. L. Pruskin, J. W. Gilje, *J. Am. Chem. Soc.* **105**, 6749 (1983).
14. It is unclear whether $Cp_2Ta(O)(CH_3)$ exists as a discrete monomer or as a mixture of linear or cyclic oligomers containing –(–Ta–O–Ta–O–)– bonds. It is apparent in the ^1H NMR spectrum that a sample of $Cp_2Ta(O)(CH_3)$ warmed above room temperature has resonances that broaden before precipitation of an intractable pale yellow powder occurs, characteristic of this kind of polymerization. Also, mass spectral analysis of **6** shows minor peaks at mass-to-charge (m/z) values that correspond to a dimeric form with the most intense peaks appearing at an m/z value consistent with the monomer.
15. The analogous pentamethylcyclopentadienyl complex has been prepared: L. L. Whinnery, L. M. Henling, J. E. Bercaw, *J. Am. Chem. Soc.* **113**, 7575 (1991).
16. NMR data for $Cp_2Ta(\mu\text{-}C_3H_3)(\mu\text{-}CO)Re_2(CO)_8$ (**4**): ^1H NMR (THF-d_8): δ 5.27 (10H, s, Cp); and 3.01 (3H, s, CH_3). ^{13}C NMR (THF-d_8): δ 266.53 (s, μ-CO); 200.57 (s, CO); 197.65 (s, CO); 197.40 (s, CO); 139.69 (m, $^3J_{CH} = 6.0$, $^1J_{CC} = 101.4$, and $^2J_{CC} = 5.0$, Ta–C–Re); 127.74 (m, $^1J_{CC} = 101.4$ and $^2J_{CH} = 8.0$, C–Me); 102.35 (m, $^1J_{CH} = 178$, $^2J_{CH} = 7.0$, and $^3J_{CH} = 6.0$, Cp); and 18.71 (m, $J_{CH} = 128.8$ and $^2J_{CC} = 5.0$, CH_3).
17. We are grateful to the National Science Foundation (grant CHE-9113261) for financial support of this work. We thank F. J. Hollander, director of the U.C. Berkeley x-ray diffraction facility (CHEXRAY), for determination of the x-ray structures.

8 September 1992; accepted 17 November 1992

Shock Amorphization of Cristobalite

A. J. Gratz, L. D. DeLoach, T. M. Clough, W. J. Nellis

Shock amorphization of cristobalite is reported and related to shock metamorphism of quartz, both being silicon dioxide polymorphs. Whereas amorphization of quartz takes place over a broad pressure range and is complete only at 35 to 40 gigapascals (350 to 400 kilobars), amorphization of cristobalite was complete (greater than 99.9 percent) by 28 gigapascals with a relatively sharp phase transformation; lower shock pressures up to 23 gigapascals resulted in no significant amorphization. Also, unlike quartz, there was no sign of lamellar amorphization, which is common in shock compression. Cristobalite amorphization should prove a useful indicator of shock pressure and is the first case of pressure amorphization of isochemical polymorphs. The diaplectic glass that is produced has a refractive index and density essentially identical to those of the diaplectic glass made from quartz, which suggests that both polymorphs collapse during shock to similar disordered phases.

Phase and microstructural changes induced by shock compression are of interest both in high-pressure physics and in studies of meteorite impacts. Materials undergoing such changes provide information about the nature of high-pressure phase transformations and about possible deformation mechanisms in minerals. For example, shock transformation and deformation of SiO_2 quartz have been studied extensively (*1–5*). When shocked to pressures of 15 to 40 GPa, the mixed-phase region (*6*), quartz transforms continuously to a disordered phase without evidence of melting (a diaplectic glass), such as flow features and loss of original grain structure. Diaplectic glass in shocked quartz is formed in the solid state in lamellar regions, usually along crystallographic directions (*7, 8*). Completion of the process at high shock pressures causes the formation of an amorphous material. A similar process occurs in the static compression of quartz in a diamond-anvil cell (*9, 10*).

Shock effects observed in various initial forms of SiO_2 in the laboratory might serve as useful indicators of shock-induced effects and pressures in nature. Notably, shock-induced microstructures in quartz can be observed with an optical microscope as planar deformation features (PDFs) and are used extensively to identify shock metamorphism. At the Cretaceous-Tertiary boundary, for example, quartz grains were shown to contain PDFs attributed to shock loading caused by meteorite impact (*11*). In addition, the extent of SiO_2 amorphization is used to estimate shock pressures, with total amorphization assumed to occur between 35 and 40 GPa, based on the quartz results.

Although shock-induced amorphization has now been observed in a variety of crystals (*12–14*), shock experiments have not been done on polymorphs of the same silicate. For SiO_2, for example, it is important to know to what extent observed phase

---

A. J. Gratz and W. J. Nellis, Institute of Geophysics and Planetary Physics and H Division, Lawrence Livermore National Laboratory, University of California, Livermore, CA 94550.
L. D. DeLoach, Y Division, Lawrence Livermore National Laboratory, University of California, Livermore, CA 94550.
T. M. Clough, Department of Chemistry, Arizona State University, Tempe, AZ 85287.

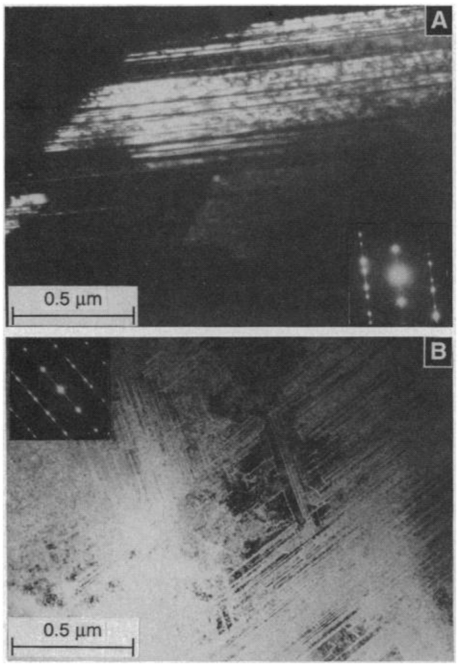

Fig. 1. Microstructure of cristobalite (**A**) before shock and (**B**) after 11.3-GPa loading. Both samples display polysynthetic (101) reflection twinning with twin lamellae as thin as a few nanometers. Diffraction patterns (insets) show corresponding streaking from the dense twinning.

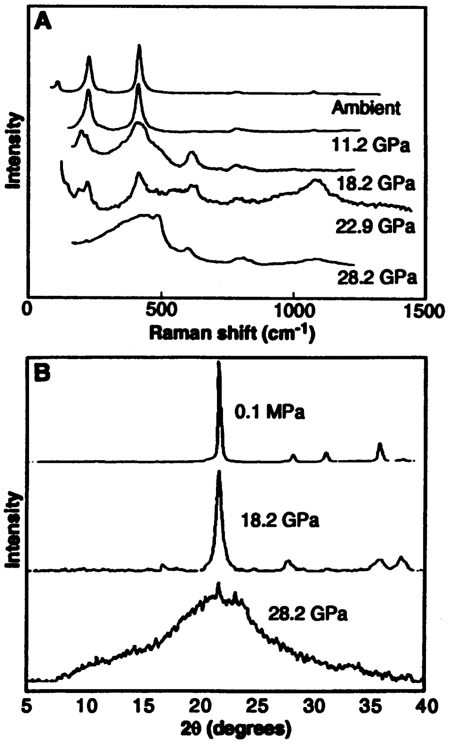

Fig. 2. (**A**) Raman spectra and (**B**) XRD patterns of samples. Both Raman and XRD show only a broadening and weakening of the signals, with no significant line shifts or evidence of amorphization, below 28.2 GPa. The highest pressure sample (>28.2 GPa) has an amorphous XRD pattern and broad Raman lines, typical of pressure glasses.

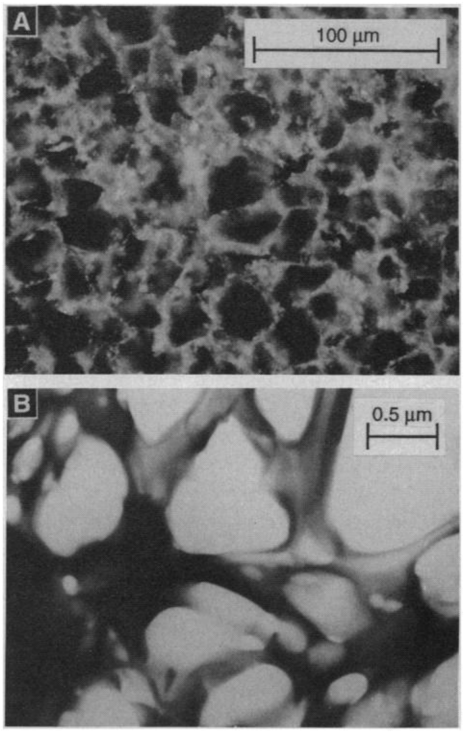

Fig. 3. Optical and TEM micrographs of a sample shocked to 28.2 GPa. The aggregate consists of (**A**) grains of diaplectic glass (black in crossed polarizing filters) separated by a bubbly fusion glass (white). At high magnification (**B**), the bubbly fusion glass is seen to consist of glass walls (dark) with individual voids (white), which are clearly visible. Both diaplectic glass and fusion glass yield amorphous electron diffraction patterns.

and microstructural features depend on the nature of the starting material. High-pressure phase and microstructural transformations might be easier to induce if a form of SiO$_2$ other than trigonal quartz is used. Also, a different initial SiO$_2$ phase might produce different microstructures and different crystal structures than quartz. In this regard, SiO$_2$ is an ideal material to study because specimens can be made in a variety of crystal structures. In addition to quartz, metastable cristobalite, tridymite, moganite, coesite, and stishorite are crystalline polymorphs of SiO$_2$, all of which can be stabilized at ambient temperature. Cristobalite in particular is found in volcanic rocks, lunar rocks and meteorites, and low-temperature siliceous deposits; devitrification of silica glasses almost always produces cristobalite. Thus, understanding the behavior of tetragonal-phase cristobalite during hypervelocity impact is useful for the interpretation of many natural phenomena and of the quenching of high-pressure phase transformations.

In this report, we present results of shock recovery experiments on α-cristobalite, a phase which has a stability range of 1743 to 1996 K at room pressure. The cubic β-phase reverts to the tetragonal metastable α-phase on cooling below 541 K. Because cristobalite is not available as large single crystals or aggregates, we performed our experiments on size-sorted powders. The unusually pure cristobalite was prepared by Phelps Freeborn at the University of California at Los Angeles by firing silica gel at 1273 K (*15*). The resultant powder contained highly twinned crystals (Fig. 1) with a domain size of about 40 nm and no other detectable phases (Fig. 2). Some large grains consisted of clusters of microcrystallites with a grain size of 0.1 to 1 µm. The observed twins were polysynthetic on the crystallographic (101) axis.

Powder specimens were shocked to high pressures with a 6.5-m-long two-stage light-gas gun as described previously (*8*). All specimens were initially at room temperature. Powder aliquots were tamped into a disk, 10 mm in diameter and 0.1 to 0.5 mm thick, that was contained in a stainless steel recovery capsule. The average initial density was 62%. Powders with particle sizes of 20 to 30 µm were shocked to 11.2, 11.3, and 22.9 GPa; 38- to 53-µm powders were shocked to 18.6 and 28.2 GPa. Specimens reached the impact pressure by a reverberating shock wave with up to about 50% of the final pressure achieved with the first shock wave (*8*, *16*). Specimens recovered after shock were remarkably homogeneous on an optical scale; initial powder size had no significant effect on the measured properties. Because deformation of shocked minerals is critical to the assignment of stress levels in impactites and to the characterization of possible phase transformations, recovered specimens were characterized with a wide range of techniques: flat-stage optical microscopy, x-ray diffraction (XRD), transmission electron microscopy (TEM), scanning electron microscopy (SEM), spindle-stage microrefractometry, and Raman spectroscopy (*17*).

Up to 22.9 GPa, specimens essentially retained their initial crystalline XRD and Raman spectra (Fig. 2) and were birefringent, having two indices of refraction. Unlike quartz (*18*), cristobalite displayed no important Raman line shifts throughout this range, and no distinctive shock-induced features were seen at these relatively low pressures. Extensive TEM study showed that no significant quantity of glass was present; however, a possible increase in twin density (Fig. 1) and extreme lattice bending of several degrees per micrometer may account for the decreased intensity and line broadening in the XRD and Raman spectra. Refractive index was also unchanged up to 18.2 GPa. We did detect a

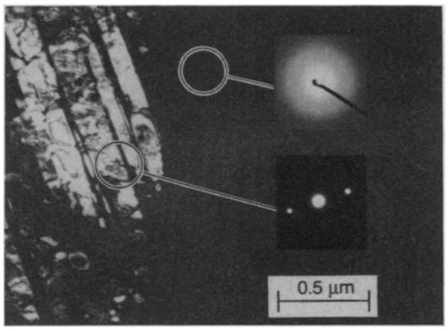

Fig. 4. Glass-crystal contact in a sample that was shocked to 28.2 GPa. Amorphous diffraction patterns from adjacent areas (insets) show the sharp contrast between regions separated by only a few hundred nanometers, without the glass lamellae that typify shock amorphization in quartz.

lowering of refractive index from 1.4848 to 1.4646 at 22.9 GPa, which was not seen at lower pressure; because no significant amount of an amorphous phase was seen in TEM, we attribute this change to intracrystalline deformation coupled with minor glass production.

In contrast to the samples at lower pressures, the specimen shocked to 28.2 GPa was almost completely amorphous, with <0.1% crystalline material left. It consisted of grains of diaplectic glass of the same size and shape as the starting cristobalite, separated by thin layers of bubbly melt glass (Fig. 3). This specimen had a broad and weak glass peak in XRD at $2\theta \approx 21°$ (Fig. 2B), which corresponds to an interplanar lattice spacing of about 0.40 nm. A study with SEM showed that this sample was almost fully dense (97%). Both diaplectic and melt glasses yielded amorphous electron diffraction patterns with no evidence of nanocrystalline domains in TEM. The resultant compact was estimated from TEM and SEM to be 86% diaplectic glass, 11% melt glass, and 3% porosity in the form of interparticle bubbles. The bulk density of 2.263×10^{-3} kg m^{-3}, measured by Archimedes principle, is close to the value of 2.33×10^{-3} kg m^{-3} for unshocked cristobalite.

Observations showed that the amorphization process in powdered cristobalite differs significantly from that in quartz. Lamellar amorphization, a process in which quartz yields the characteristic PDFs, was not observed in shocked cristobalite. No distinctive shock-induced deformation features were seen in the shocked, but still crystalline, cristobalite grains, although some shock features would be difficult to image because of the high twin density. Instead, relict crystalline regions in the highly shocked specimen were in intimate contact with homogeneous glass (Fig. 4). Cristobalite amorphization did not follow twin boundaries, as in feldspars (*19*), which suggests that the twin strain energy does not strongly influence amorphization. Complete amorphization occurred at lower pressures in cristobalite (about 25 GPa) than in quartz (35 to 40 GPa). Also for cristobalite, the range of pressures that the mixed-phase region spanned is substantially less than for quartz. The transformation from cristobalite to glass occurred somewhere between 22.9 and 28.2 GPa, which means that the region of transformation may be even more narrow than these limits. In contrast, the mixed-phase region for quartz is between about 15 and 40 GPa.

Despite these differences, the diaplectic glasses produced by shock of cristobalite and quartz have very similar properties. Refractive indices n and densities ρ of the quartz and cristobalite diaplectic glasses were very nearly identical ($n = 1.460$ to 1.464 versus $n = 1.4685 \pm 0.0004$; $\rho = 2.219$ to 2.261 versus $\rho = 2.3 \pm 0.1$, respectively) (*20–22*), whereas the corresponding values for the two crystalline polymorphs, from which the glasses originated, differed significantly ($n = 1.5440$ to 1.5453 versus $n = 1.484$ to 1.487; $\rho = 2.65$ versus $\rho = 2.33$, respectively). Moreover, diaplectic cristobalite had a broadened Raman spectrum quite similar to spectra of quasi-statically compressed quartz, coesite, and glass (*23*). Similarities included D_1 and D_2 defect bands at about 500 and 620 cm^{-1} and a glass peak at about 800 cm^{-1}. Thus, although pressure amorphization can be reversible or yield materials with varying degrees of memory of their precursors (*24–26*), diaplectic glass produced from quartz or cristobalite has only a small memory of its initial properties. Put another way, there is no evidence that different crystalline silica polymorphs collapse to different glasses. Both quartz and cristobalite probably collapse to similar disordered phases during shock loading.

We have shown that shock amorphization occurs in more than one silica polymorph. The high-pressure phase transformations in shocked powdered cristobalite and crystalline quartz differ in the value of the amorphization pressure, the width of the mixed-phase region, and the microstructures of the recovered specimens. Our results also suggest that diaplectic silica glass found in nature may not always result from shocked quartz; it may come from shocked cristobalite or even from other silica polymorphs. Thus, determination of the shock behavior of other silica polymorphs is also important. Because identification of the precursor cannot be made on the basis of refractive index alone, petrographic analysis is required. In general, rock type and mineral associations are sufficient to identify the precursor silica phase of the parent rock. Without this detailed analysis, however, interpreted shock stresses could be in considerable error because of pressure differences required to amorphize different silica polymorphs.

REFERENCES AND NOTES

1. P. S. De Carli and J. C. Jamieson, *J. Chem. Phys.* **31**, 1675 (1959).
2. P. S. De Carli and D. J. Milton, *Science* **147**, 144 (1965).
3. E. C. T. Chao, *ibid.* **156**, 192 (1967).
4. W. F. Müller and M. Defourneaux, *Z. Geophys.* **34**, 483 (1968).
5. F. Langenhorst, A. Deutsch, D. Stöffler, U. Hornemann, *Nature* **356**, 507 (1992).
6. D. E. Grady, W. J. Murri, G. R. Fowles, *J. Geophys. Res.* **29**, 332 (1974).
7. A. J. Gratz, J. Tybruczy, J. Christie, T. Ahrens, P. Pongratz, *Lunar Planet Sci. XIX*, 421 (1988).
8. A. J. Gratz *et al.*, *Phys. Chem. Miner.* **19**, 267 (1992).
9. R. J. Hemley, A. P. Jephcoat, H. K. Mao, L. C. Ming, M. H. Manghnani, *Nature* **334**, 52 (1988).
10. K. J. Kingma, R. J. Hemley, C. Meade, H. K. Mao, D. R. Veblen, *Science* **259**, 666 (1993).
11. B. F. Bohor, E. E. Foord, P. J. Modreski, D. M. Triplehorn, *ibid.* **224**, 867 (1984).
12. O. Mishima, L. D. Calvert, E. Whalley, *Nature* **310**, 393 (1984).
13. J. Arndt, in *Shock Waves in Condensed Matter, 1983*, J. R. Asay, R. A. Graham, G. K. Straub, Eds. (Elsevier, New York, 1985), p. 473.
14. A. L. Chen, P. Y. Yu, M. P. Pasternak, *Phys. Rev. B* **44**, 2883 (1991).
15. This sample was produced outside the cristobalite stability field for unknown kinetic reasons; tridymite has also been found to transform to cristobalite at room pressure below 1743 K [T. Arahori and T. Suzuki, *J. Mater. Sci.* **22**, 2248 (1987)]. The twins are probably attributable to cooling through the α-β transformation.
16. All shock recovery experiments are of the ring-up type. The powder specimen is compressed by a shock wave that reverberates through the specimen between steel walls. For the particular case of powders, heating is probably produced by intergranular friction. However, it is well known from modeling and experiments [for example, W. H. Gourdin, *Metall. Trans. A* **15**, 1653 (1984); R. B. Schwarz *et al.*, *Acta Metall.* **32**, 1243 (1984)] that this only results in localized heating of a thin skin of particles on the surface, with melting limited to <1 μm in SiO_2 [K. I. Kondo, S. Soga, A. Sawaoka, M. Araki, *J. Mater. Sci.* **20**, 1033 (1985)], in agreement with our observations of small quantities of intergranular melting.
17. Phase changes were studied by XRD with Cu-Kα radiation. Flat-stage optical microscopy and SEM, at 15 keV on a SEMCO Nanolab VII, provided details of sample texture and birefringence. We performed TEM at 200 keV on a Jeol 200CX (point-to-point resolution of 0.25 nm) with a Kevex EDS system for chemical analysis and a defocused beam to minimize radiation damage. Microrefractometry (to determine index of refraction) was on a heated spindle stage constructed at the Lawrence Livermore National Laboratory with Hg 546-nm illumination. Raman spectra were obtained with an Instruments S.A. triple spectrometer (S3000) coupled with a Princeton Instruments intensified diode-array detector (IY-750) for multichannel detection. Sample excitation was induced with the use of the 488-nm line of a Coherent (90-5). Laser focusing and signal collection were performed with a long working distance Mitutoyo ×50 objective (numerical aperture 0.40). This objective and other focusing and collection optics were built around a modified Olympus BH-2 petrographic microscope. Polarized spectra were obtained in the backscattering geometry, and a grating with 600 grooves per millimeter was used.

18. P. F. McMillan, G. H. Wolf, P. Lambert, *Phys. Chem. Miner.* **19**, 71 (1992).
19. E. C. T. Chao *et al.*, *Proc. Apollo 11 Lunar Sci. Conf. I* (1970), p. 287.
20. W. v. Engelhardt *et al.*, *Contrib. Mineral. Petrol.* **15**, 93 (1967).
21. D. Stöffler, *Fortschr. Mineral.* **51**, 256 (1974).
22. Refractive indices reported in literature do not generally list the wavelength of light used for the measurement. Silica phases have small dispersions which lead to variations of <0.005 in the refractive index at typical wavelengths. Our measured values will tend to be somewhat (~0.002) higher than those using the Na 589-nm line.
23. R. J. Hemley, in *High Pressure Research in Mineral Physics*, M. H. Manghnani and Y. Syono, Eds. (Mineral Physics Series, American Geophysical Union, Washington, DC, 1987), vol. 2, p. 347.
24. M. B. Kruger and R. Jeanloz, *Science* **249**, 647 (1990).
25. L. E. McNeil and M. Grimsditch, *Phys. Rev. Lett.* **68**, 83 (1992).
26. R. R. Winters, G. S. Serghiou, W. S. Hammack, *Phys. Rev. B* **46**, 2792 (1992).
27. Gas-gun experiments were performed by N. A. Hinsey. We thank M. Wall for help with TEM, W. Beiriger for XRD, V. Chin for photodeveloping, and especially M. L. Olsen for help with TEM analyses. All of this work, done at the Lawrence Livermore National Laboratory, was performed under the auspices of the U.S. Department of Energy under contract W-7405-ENG-48.

17 September 1992; accepted 16 December 1992

Microstructural Observations of α-Quartz Amorphization

Kathleen J. Kingma, Charles Meade, Russell J. Hemley,
Ho-kwang Mao, David R. Veblen

Solid-state amorphization is a transformation that has been observed in a growing number of materials. Microscopic observations indicate that amorphization of α-quartz begins with formation of crystallographically controlled planar defects and is followed by growth of amorphous silicon dioxide at these defect sites. Similar transformation microstructures are found in quartz upon quasihydrostatic and nonhydrostatic compression in a diamond-anvil cell to 40 gigapascals and from simple comminution. The results suggest that there is a common mechanism for solid-state amorphization of silicates in static and shock high-pressure experiments, meteorite impact, and deformation by tectonic processes. In general, these results are consistent with recently proposed shear instability models of amorphization.

The phases of silica are important for a wide range of problems in materials science, solid-state physics, and geology (*1*). The formation, stability, and physical properties of the amorphous forms in this system are of particular importance because of their technological applications and the role of silica glass as an archetypal noncrystalline material. Besides conventional melt quenching, amorphous silica can be synthesized from α-quartz by several solid-state processes that include the application of static high pressures (*2, 3, 4*), comminution (*5*), and shock compression (*6, 7, 8*).

There is now great experimental and theoretical interest in the solid-state crystalline-amorphous transitions of silica and a range of other compounds. Much of the work in this area focuses on descriptions of individual pressure-induced transitions and identification of the similarities they have with conventional phase transitions (such as melting and crystalline-crystalline transitions). To date, there have been a large number of experimental observations of amorphization in different materials (*9*). Despite these observations and the theoretical simulations of amorphization [particularly for SiO_2 (*10*)], a detailed characterization of this transformation is still lacking. Such information is crucial to test recent theoretical models of the transition from crystalline to amorphous states (*10*).

To address these issues, one must determine the manner in which the amorphous phase nucleates, the scale of sample heterogeneity during the transition, and the extent of disordering over a broad range of length scales. Only transmission electron microscopy (TEM) can provide such information because it allows simultaneous imaging and diffraction information at the unit-cell level. Despite these advantages, TEM examination of quench products from diamond-anvil cell experiments is complicated because of the difficulty in handling the small samples and the instability of metastable high-pressure phases under the electron beam. Recently, we have developed experimental techniques to allow routine TEM observations of diamond-cell samples, and here we combine these methods with spectroscopic and optical observations to document the amorphization of α-quartz over four orders of magnitude in length scales.

We examined the transformation mechanism between crystalline and amorphous phases by synthesizing samples of coexisting crystalline and noncrystalline SiO_2 over a wide range of stress conditions. In high-pressure experiments, samples of natural quartz were compressed in the diamond cell under quasihydrostatic and nonhydrostatic conditions (*11*). Phase transformations were monitored with in situ micro-Raman techniques (*3*). Samples were then decompressed from maximum pressure of 15 to 40 GPa to quench the high-pressure transformation microstructures. In comminution experiments, natural quartz was initially ground in a mullite mortar and pestle. After sieving, we ground grains <43 μm (325 mesh) in a ball-milling machine (*12*). The recovered samples from all experiments were characterized by Raman spectroscopy and by optical and electron microscopy (*13*).

TEM images and electron-diffraction patterns showed complete amorphization with no sign of residual crystallinity for diamond-cell samples that were recovered from the highest pressures (>30 GPa). This observation confirms that the loss of sharp diffraction and Raman spectra in previous high-pressure studies (*2, 3*) was due to amorphization; it was not the result of crystallite size reduction of the parent quartz. In samples that have been either ground or quenched from between 15 and 30 GPa (Fig. 1), the amorphous phase formed in the parent crystalline structure with a characteristic lamellar habit, growing at planar defect sites. As these lamellae grew in size, they maintained subplanar contacts with the crystal, having the same orientation as the original defect. Compared to that of the ground samples, the density of planar features (planar defects and amorphous lamellae) was higher in samples that were quenched from polycrystalline diamond-cell experiments and appeared to rise with increasing maximum pressure. However, detailed examination of a large number of grains from a series of different experiments indicates that the microstructures that were formed by grinding and by static compression are indistinguishable by TEM. The lack of high-temperature effects (such as recrystallization, flow texture, and diffuse boundaries) indicates that the glass lamellae were formed from a solid state transformation; they are not melt-quenched features. In all samples, the planar defects and amorphous lamellae were parallel to rational crystallographic planes. To date, we have found planar features in {001}, {100}, {101}, $\{0\bar{1}1\}$, {102}, $\{20\bar{1}\}$,

---

K. J. Kingma, Geophysical Laboratory and Center for High Pressure Research, Carnegie Institution of Washington, Washington, DC 20015, and Department of Earth and Planetary Sciences, The Johns Hopkins University, Baltimore, MD 21218.
C. Meade, R. J. Hemley, H.-k. Mao, Geophysical Laboratory and Center for High Pressure Research, Carnegie Institution of Washington, Washington, DC 20015.
D. R. Veblen, Department of Earth and Planetary Sciences, The Johns Hopkins University, Baltimore, MD 21218.